Atomic Scale Mechanism of the Transformation of γ-Alumina to θ-Alumina

Shu-Hui Cai,[1,2] Sergey N. Rashkeev,[3] Sokrates T. Pantelides,[3,4] and Karl Sohlberg[2,*]

[1]*Department of Physics, State Key Laboratory for Physical Chemistry of Solid Surface, Xiamen University, Xiamen 361005, People's Republic of China*

[2]*Department of Chemistry, Drexel University, Philadelphia, Pennsylvania 19104*

[3]*Department of Physics, Vanderbilt University, Nashville, Tennessee 37235*

[4]*Solid State Division, Oak Ridge National Laboratory, Oak Ridge, Tennessee 37831*

(Received 17 April 2002; published 13 November 2002)

γ-alumina is known to transform to θ-alumina and finally to α-alumina upon thermal treatment with a catastrophic loss of porosity and catalytic activity. First-principles calculations were performed to investigate the atomic scale mechanism of the γ- to θ-alumina transformation. The transformation pathways between the two different forms have been mapped out and identified as a sequence of Al cation migrations. Different possible Al migration paths may be responsible for the experimentally observed formation of domains and twins in θ-alumina. The estimated temperature dependence of the conversion rate is in excellent agreement with the experimental transformation temperature.

DOI: 10.1103/PhysRevLett.89.235501 PACS numbers: 61.50.Ks, 63.70.+h, 64.60.–i, 64.70.Kb

Alumina, nominally Al_2O_3, is an exceptionally significant structural and functional ceramic material. Besides the thermodynamically stable α-alumina (corundum) form, it exists in many metastable forms (transition aluminas), which are widely used in catalysis, microelectronics, optics, etc. [1–3]. These have been the subject of many experimental and theoretical investigations [1–7]. The transition aluminas are derived by thermal dehydration of aluminum hydroxide precursors. The dehydration sequence, boehmite $\rightarrow \gamma \rightarrow \delta \rightarrow \theta \rightarrow \alpha$, is of particular interest since γ-alumina is one of the most important catalytic support materials. One serious industrial problem is that at elevated temperatures, undoped γ-alumina transforms rapidly to α-alumina, accompanied by a catastrophic loss of porosity via sintering. An understanding of the mechanisms of the polymorphic phase transformations would therefore be of great value in developing improved material preparation for control of sintering, and therefore retention of porosity.

In this Letter, we report a theoretical study of the atomic scale mechanism of the phase transition from γ- to θ-alumina (δ-alumina is viewed as a superstructure of γ-alumina [8]), the critical first step leading to loss of porosity. The transformation leads to loss of porosity in two ways. First, the product θ-alumina is intrinsically a lower surface-area material than γ-alumina [4]. Second, the unit cell of θ-alumina is a defect-free structure, whereas the unit cell of γ-alumina must contain defects. To the best of our knowledge, there are just a few previous theoretical works related to the transformation of γ- to θ-alumina [5,8], which proposed a space group sequence analysis to depict possible transformation paths based on symmetry group/subgroup relationships. The phase transformation mechanism proposed here correctly predicts the observed orientation relationship between γ- and θ-alumina, and reveals the origin of the observed interfaces in domain boundaries in θ-alumina. The predicted rate of the thermal conversion is in excellent agreement with the well-established experimental value.

The calculations were based on density functional theory and employed the generalized gradient approximation to the exchange-correlation energy. Ultrasoft pseudopotentials [9] have been used. A plane wave basis set has been used to describe the electronic wave functions with a cutoff energy of 380 eV, and two special k points in the Monkhorst-Pack integration scheme have been employed [10]. The Al vibrational frequencies are harmonic [11].

γ-alumina is known to have a defect cubic spinel structure ($Fd\bar{3}m$) [4,12,13] with Al cations distributed over the octahedral (O_h) and tetrahedral (T_d) interstitial sites defined by the oxygen anion sublattice. The 8/3 cation vacancies per cubic unit cell are required to maintain the Al_2O_3 stoichiometry. Starting from the defect-free spinel structure (AB_2O_4), we first constructed a unit cell $Al_{18}O_{24}$ [Fig. 1(a)] in terms of the basis vectors of its cubic cell $\boldsymbol{a}_\gamma$, $\boldsymbol{b}_\gamma$, and $\boldsymbol{c}_\gamma$, such that $\boldsymbol{a}_{\gamma\mathrm{N}} = 1.5\boldsymbol{a}_\gamma + 0.5\boldsymbol{b}_\gamma$, $\boldsymbol{b}_{\gamma\mathrm{N}} = -0.5\boldsymbol{b}_\gamma + 0.5\boldsymbol{c}_\gamma$, $\boldsymbol{c}_{\gamma\mathrm{N}} = -0.5\boldsymbol{b}_\gamma - 0.5\boldsymbol{c}_\gamma$, where $\boldsymbol{a}_{\gamma\mathrm{N}}$, $\boldsymbol{b}_{\gamma\mathrm{N}}$, and $\boldsymbol{c}_{\gamma\mathrm{N}}$ are the unit vectors of the redefined cell. The two vacancies can then be assigned to any positions among the 18 cation sites to satisfy the Al_2O_3 stoichiometry. The constructed cell (γ_N) is one of the minimal possible cells that contain an integer number of cation vacancies.

Full geometry optimization indicates that the total energy increases with decreasing distance between the two vacancy sites, in accordance with the conclusion of Wolverton and Hass [7]. In the lowest energy configuration, the vacancies are located in $\{1\bar{1}\bar{1}\}_{\gamma\mathrm{N}}$ planes, (i.e., in $\{110\}_\gamma$ planes), in agreement with the high-resolution electron microscopy observations [14,15].

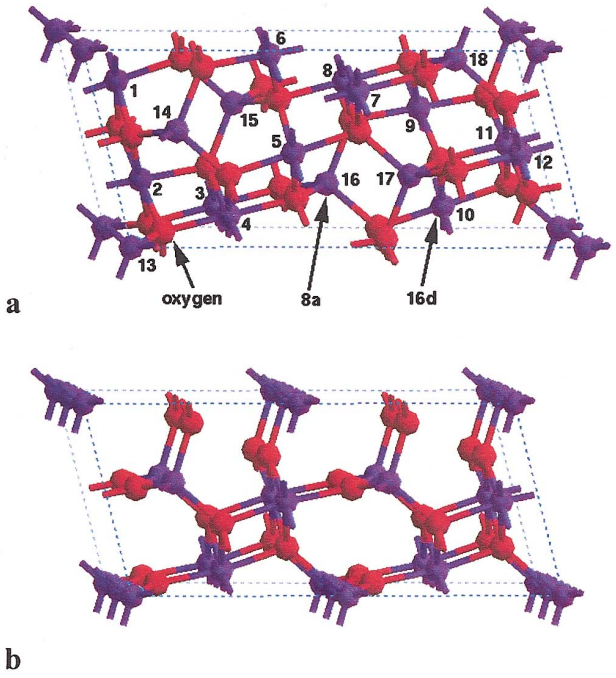

FIG. 1 (color). (a) Vacancy-free cell of γ-alumina defined by $\boldsymbol{a} = 1.5\boldsymbol{a}_\gamma + 0.5\boldsymbol{b}_\gamma$, $\boldsymbol{b} = -0.5\boldsymbol{b}_\gamma + 0.5\boldsymbol{c}_\gamma$, $\boldsymbol{c} = -0.5\boldsymbol{b}_\gamma - 0.5\boldsymbol{c}_\gamma$. (b) Supercell of θ-alumina defined by $\boldsymbol{a}_{\theta_N} = \boldsymbol{a}_\theta - \boldsymbol{b}_\theta$, $\boldsymbol{b}_{\theta_N} = 2\boldsymbol{b}_\theta$, $\boldsymbol{c}_{\theta_N} = \boldsymbol{c}_\theta$, and translation of cell origin (red spheres: oxygen; purple spheres: aluminum). The similarity between these two structures is apparent.

θ-alumina is monoclinic with space group $C2/m$. There are four formula units per unit cell with all of the ions located at 4i Wyckoff positions [12,13].

Although the structures of γ- and θ-alumina look rather different (cubic and monoclinic symmetry, respectively), both have an fcc oxygen anion sublattice with Al cations occupying a portion of the available O_h and T_d interstices. Examination of the θ structure reveals that it can be redefined to a shape very similar to that of γ_N, by enlarging the θ-alumina primitive unit cell Al_8O_{12} to a cell $Al_{16}O_{24}$ [cell θ_N, Fig. 1(b)] using new unit vectors $\boldsymbol{a}_{\theta_N} = \boldsymbol{a}_\theta - \boldsymbol{b}_\theta$, $\boldsymbol{b}_{\theta_N} = 2\boldsymbol{b}_\theta$, $\boldsymbol{c}_{\theta_N} = \boldsymbol{c}_\theta$, where $\boldsymbol{a}_\theta$, $\boldsymbol{b}_\theta$, and $\boldsymbol{c}_\theta$ are the basis vectors of θ-alumina. The only essential difference between γ_N and θ_N is in the distribution of Al atoms in the interstices among the oxygen sublattice.

There are two *direct* pathways that transform cell γ_N into a unit cell similar to θ_N (here "direct" implies that Al atoms move to adjacent unoccupied T_d or O_h sites), which give us two ways to construct a model θ-alumina cell from the redefined cell γ_N.

Scheme A: The transformation is achieved by keeping two 8a and six 16d Al atoms at their original sites, and moving the remaining eight Al atoms to two 16c and six 48f sites (below we call the product of this scheme model A).

Scheme B: The transition is reached by keeping two 16d Al atoms at their original places. All the 14 other Al atoms move to six 16c, two 8b, and six 48f sites (we call the product of this scheme model B).

The resulting models are shown in Fig. 2. For easier comparison, two unit cells are shown and the Al atoms in different T_d and O_h sites are represented by different colors. Disregarding the small distortion, models A and B are translationally equivalent, with the translation vector $\boldsymbol{R} = \boldsymbol{c}_{\gamma N}/2$ (Fig. 2). Also, both models A and B can each be constructed in three equivalent ways, depending on different sets of the occupied 8a and 16d sites. The three A (or B) variants of the model can be approximately generated by translating model A (or B) on the vectors as follows: $\boldsymbol{R} = \boldsymbol{a}_{\gamma N}/6 - \boldsymbol{b}_{\gamma N}/6 + \boldsymbol{c}_{\gamma N}/3$ and $\boldsymbol{R} = \boldsymbol{a}_{\gamma N}/3 + \boldsymbol{b}_{\gamma N}/6 + 2\boldsymbol{c}_{\gamma N}/3$. If the oxygen anions of γ-alumina are in ideal positions (i.e., the μ of the oxygen fractional coordinate (μ, μ, μ) is 0.375, instead of the practical value 0.387), the constructed θ models can be further simplified to Al_8O_{12} with the cell in the shape of θ-alumina reported experimentally.

Based on the relationship between the γ_N-alumina and γ-alumina lattice axes, we can establish the orientation

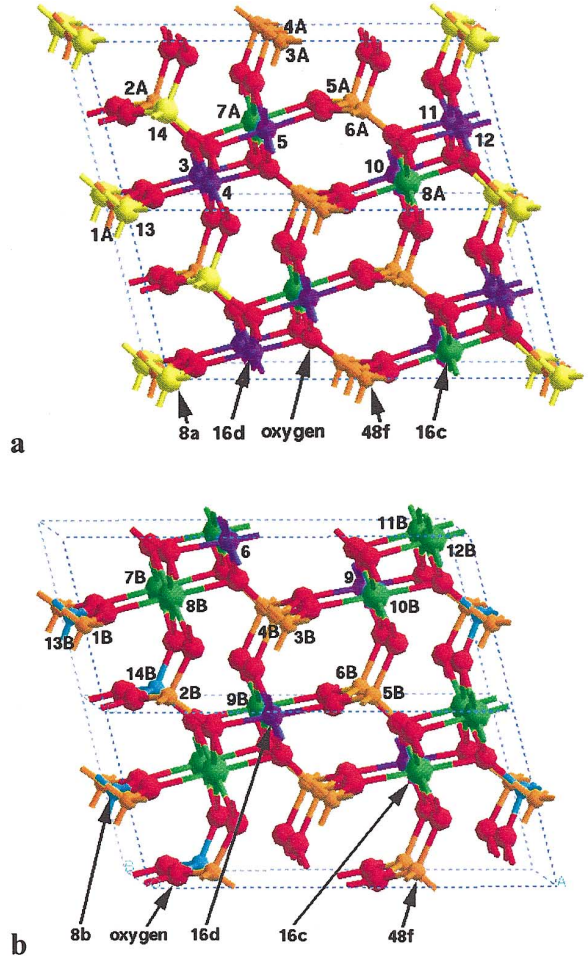

FIG. 2 (color). Two θ-models produced from γ-alumina by different transformation schemes: (a) Model A; (b) Model B. Note the translational relationship $\boldsymbol{R} = \boldsymbol{c}_\theta/2$ between the two models.

relations between γ-alumina and θ-alumina models as follows: $[010]_\theta \parallel [0\bar{1}1]_\gamma$ and $(100)_\theta \parallel (100)_\gamma$. According to lattice symmetries, they are exactly equivalent to the experimental results of $[010]_\theta \parallel [110]_\gamma$ and $(100)_\theta \parallel (001)_\gamma$ [5,8].

The two θ models and the experimental θ-alumina structure are essentially identical upon full geometry optimization from first principles (Table I) [12]. The energy difference between them is less than $0.002\,\mathrm{eV}/\mathrm{Al_2O_3}$. The optimized lattice parameters are consistent with earlier theoretical calculations on θ-alumina [7]. As $\boldsymbol{a}_{\gamma\mathrm{N}} = \boldsymbol{a}_\theta - \boldsymbol{b}_\theta$, $\boldsymbol{b}_{\gamma\mathrm{N}} = 2\boldsymbol{b}_\theta$, and $\boldsymbol{c}_{\gamma\mathrm{N}} = \boldsymbol{c}_\theta$, the translational relations among the variants of the θ model (there are three variants for each model) can be converted to $\boldsymbol{R} = \boldsymbol{c}_\theta/2$, $\boldsymbol{R} = \boldsymbol{a}_\theta/6 - \boldsymbol{b}_\theta/2 + \boldsymbol{c}_\theta/3$, $\boldsymbol{R} = \boldsymbol{a}_\theta/6 - \boldsymbol{b}_\theta/2 - \boldsymbol{c}_\theta/6$, $\boldsymbol{R} = \boldsymbol{a}_\theta/3 + 2\boldsymbol{c}_\theta/3$, and $\boldsymbol{R} = \boldsymbol{a}_\theta/3 + \boldsymbol{c}_\theta/6$.

There are five possible nonequivalent fundamental steps in the migration of a Al cation from its original interstitial site to a neighboring interstitial site related to the γ-alumina to θ-alumina transformation: (i) $8a$ to $16c$; (ii) $16d$ to $48f$; (iii) $8a$ to $48f$; (iv) $16d$ to $16c$; and (v) $16d$ to $8b$ (only for scheme B). Taking the lowest energy configuration of γ_N cell as a start, we moved Al atoms to their destinations one by one to determine the lowest energy intermediate states of scheme A. First we moved every Al atom whose migration is required for the transformation to all of its possible destinations ($16c$ or $48f$) and selected the lowest energy step. From this new state we continued by identifying the lowest energy displacement of a second Al atom. This process was repeated until model A was established. The lowest energy transformation sequence was found to be the following: (1) $6 \rightarrow 3A$, (2) $9 \rightarrow 6A$, (3) $16 \rightarrow 4A$, (4) $15 \rightarrow 7A$, (5) $1 \rightarrow 2A$, and (6) $18 \rightarrow 1A$. Accompanying the sixth step, the last two Al atoms that should be moved to complete the γ- to θ-alumina transformation relax to their destinations spontaneously.

When calculating the transition barriers between adjacent intermediates, we successively fixed the positions of the migrating atom and one of the atoms far away from it (to avoid the "sliding" of the whole cell) and relaxed the positions of all the other atoms in the cell. The results are shown in Fig. 3. Step (4) is the real rate-controlling step.

The rate at which a given step of the transition occurs is determined by the relation

$$r = \nu f \rho(E > \Delta E),$$

where ν is the vibrational frequency with which the reactant approaches the top of the barrier, f is the population of the reactant, and $\rho(E > \Delta E)$ is the probability that the reactant has sufficient energy to surmount the barrier ΔE, i.e.,

$$\rho(E > \Delta E) = \frac{1}{kT}\int_{\Delta E}^{\infty} e^{-E/kT} dE.$$

Here k is the Boltzmann constant, and T is the Kelvin temperature. Assuming that quasiequilibria are established among all intermediates that precede the rate-controlling step (and the reactant), Boltzmann statistics were employed to estimate the population of the intermediate precursor to the rate-controlling step.

The temperature range of stability for θ-alumina in the sequence of the dehydration of boehmite is about 1200–1300 K [4]. The predicted rate for the key step at 1300 K is $1.76 \times 10^{-5}\ \mathrm{s}^{-1}$, which implies that about 11 h are required for half of the reactants to surmount the barrier, in excellent agreement with experimental reaction time (about 2–10 h) [12,16].

All calculations reported above are for scheme A. As the energy increase accompanying the migration of Al($16d$) to an $8b$ site is much higher than those of Al($16d$) to $48f$ or $16c$ sites, the transformation by scheme B is energetically less favorable. In addition, one needs to reorder 14 atoms to complete the transformation of γ- to θ-alumina by scheme B (instead of 8 atoms in scheme A), which makes this scheme statistically less probable as well. Therefore, starting from the same configuration, the transformation by scheme B will occur much more slowly than by scheme A. Of course, due to the range of distributions of Al vacancies, different Al migration paths are possible, thus forming the variants of the models A and B in different domains. This is consistent with the observed formation of twins and interfaces in θ-alumina [8,16].

Two types of domain boundaries are observed experimentally — translational and rotational. The observed translational interfaces have been reported to correspond to the translational vectors $\boldsymbol{R} = \boldsymbol{c}_\theta/2$ and $\boldsymbol{R} = \boldsymbol{a}_\theta/3$ [8,16]. The translational interface with $\boldsymbol{R} = \boldsymbol{c}_\theta/2$ can be formed by ordering cations through schemes A and B, respectively, in neighboring domains (Fig. 2) [8]. However, the translational interface

TABLE I. Optimized structural parameters of θ-alumina.

Method	a (Å)	b (Å)	c (Å)	α (°)	β (°)	γ (°)
Expt. [12]	12.13	5.733	5.532	90.00	103.5	103.7
Model A	12.20	5.727	5.529	89.85	103.7	103.8
Model B	12.22	5.719	5.529	89.90	103.6	103.8

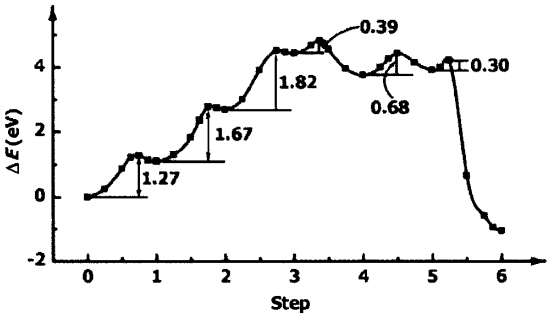

FIG. 3. Energy profile along the reaction pathway.

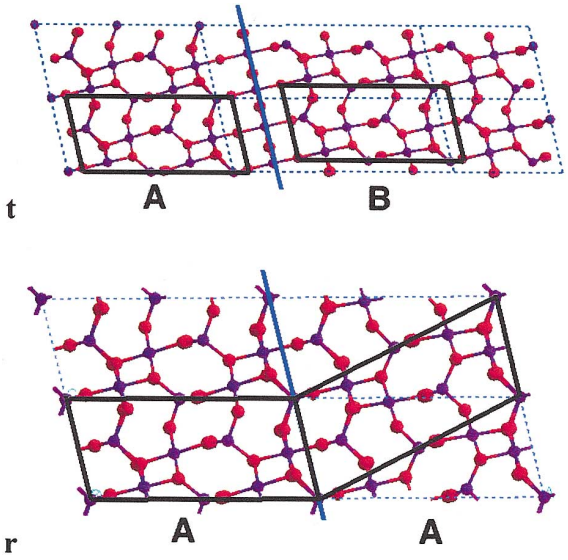

FIG. 4 (color). Models of translational and rotational interfaces in θ-alumina: (t) Translational interface with $\boldsymbol{R} = \boldsymbol{a}_\theta/3 + \boldsymbol{c}_\theta/6$; ($r$) Rotational interface with $\boldsymbol{b}_\theta$, $\boldsymbol{c}_\theta$ rotated 180° around $\boldsymbol{a}_\theta$. See Fig. 2 for $\boldsymbol{R} = \boldsymbol{c}_\theta/2$.

with $\boldsymbol{R} = \boldsymbol{a}_\theta/3$ seems incompletely identified [8]. According to the translational relationships between the variants of the θ models mentioned above, we suggest that the observed translational interface is actually $\boldsymbol{R} = \boldsymbol{a}_\theta/3 + \boldsymbol{c}_\theta/6$, with the $\boldsymbol{c}_\theta/6$ value being too small to be observed [Fig. 4(t)]. The rotational interface on $(001)_\gamma$ planes is explained by the 180° rotation of the $\boldsymbol{b}_{\gamma\mathrm{N}}$ and $\boldsymbol{c}_{\gamma\mathrm{N}}$ axes around $\boldsymbol{a}_{\gamma\mathrm{N}}$, i.e., $\boldsymbol{a}'_{\theta\mathrm{N}} = \boldsymbol{a}_{\gamma\mathrm{N}}$, $\boldsymbol{b}'_{\theta\mathrm{N}} = -\boldsymbol{b}_{\gamma\mathrm{N}}$, $\boldsymbol{c}'_{\theta\mathrm{N}} = -\boldsymbol{c}_{\gamma\mathrm{N}}$, in a neighboring domain [Fig. 4(r)] [8]. The twinned interface reported by Wang *et al.* is actually rotational plus translational [16].

To account for the extension of the lattice vector a_γ by the factor of 3/2 in the γ- to θ-alumina transformation, Levin and co-workers suggested that the process must proceed through disordering of the γ form to a simple fcc structure with a_γ reduced by 2, with subsequent reordering with a threefold increase of the lattice parameter [5,8]. Our study shows that $3/2a_\gamma$ is easily explained by the θ models constructed from the γ_N cell. Although $a_{\gamma\mathrm{N}} = (5/2)^{1/2}a_\gamma$, a_θ can be simplified to $3/2a_\gamma$ if one neglects the small distortion of oxygen sublattice. It may be true that the lattice symmetry becomes nominally $Fm\bar{3}m$ during the γ- to θ-alumina transformation process by scheme B, due to the large scale rearrangement of the Al sublattice and the involvement of the 8b sites, but it does not seem to be necessary to satisfy such a restriction in the domain where the transformation takes place by scheme A, wherein the 8b sites are not involved.

In summary, we have shown that although the unit cell of cubic γ-alumina looks quite different from that of monoclinic θ-alumina, both of them can be described by cells containing $Al_{16}O_{24}$ that are very similar. We found that when some of the Al atoms in γ-alumina move to specific sites, a structure that is a close approximant of the θ-alumina structure is formed. Two possible cation reordering schemes are proposed which eventually form translationally equivalent θ models, both of which are equivalent to the experimental structure within the margins of error of the calculations.

Based on our first-principles calculations, the Al migration is found to take place first in the vicinity of the cation vacancies in order to reduce the strong Al-Al interactions. Starting from a lowest energy configuration of γ-alumina, the lowest energy pathway of transformation was mapped out. The computed conversion rate recovers the experimental transformation temperature with high accuracy. The experimental observations of the orientation relationship between γ- and θ-alumina, and the translational and rotational interfaces in θ-alumina can be reasonably explained within the proposed models.

This work was supported in part by the U.S. DOE under Contract No. DE-FC02-01CH11085, by an NSF GOALI Grant No. DMR-0111841 with Alcoa, Inc., and by the William A. and Nancy F. McMinn Endowment at Vanderbilt University. Computations were partially supported by the National Center for Supercomputing Applications under Grant No. CHE990015Nr00.

*Email address: sohlbergk@drexel.edu

[1] H. Knözinger and P. Ratnasamy, Catal. Rev. Sci. Eng. **17**, 31 (1978).
[2] M. Che and C. O. Bennett, Adv. Catal. **36**, 55 (1989).
[3] C. N. Satterfield, *Heterogeneous Catalysis in Practice* (McGraw-Hill, New York, 1980), Sect. 4.5.
[4] K. Wefers and C. Misra, Alcoa Laboratories Technical Report No. 19, 1987.
[5] I. Levin and D. Brandon, J. Am. Ceram. Soc. **81**, 1995 (1998), and references therein.
[6] K. Sohlberg, S. J. Pennycook, and S. T. Pantelides, Chem. Eng. Commun. **181**, 107 (2000).
[7] C. Wolverton and K. C. Hass, Phys. Rev. B **63**, 024102 (2001), and references therein.
[8] I. Levin, L. A. Bendersky, D. G. Brandon, and M. Rühle, Acta Mater. **45**, 3659 (1997).
[9] D. Vanderbilt, Phys. Rev. B **41**, 7892 (1990).
[10] H. J. Monkhorst and J. D. Pack, Phys. Rev. B **13**, 5188 (1976).
[11] S. Califano, *Vibrational States* (Wiley, London, 1976).
[12] R.-S. Zhou and R. L. Snyder, Acta Crystallogr. Sect. B **47**, 617 (1991), and references therein.
[13] J. A. Wang, X. Bokhimi, A. Morales, O. Novaro, T. López, and R. Gómez, J. Phys. Chem. B **103**, 299 (1999).
[14] Y. G. Wang, P. M. Bronsveld, J. T. M. De Hosson, B. Djuricic, D. McGarry, and S. Pickering, J. Am. Ceram. Soc. **81**, 1655 (1998).
[15] G. N. Kryukova, D. O. Klenov, A. S. Ivanova, and S. V. Tsybulya, J. Eur. Ceram. Soc. **20**, 1187 (2000).
[16] Y. G. Wang, P. M. Bronsveld, J. T. M. De Hosson, B. Djuricic, D. McGarry, and S. Pickering, J. Eur. Ceram. Soc. **18**, 299 (1998).